PolarTracker: Attitude-aware Channel Access for Floating Low Power Wide Area Networks

Yuting Wang, Xiaolong Zheng, Liang Liu, Huadong Ma
Beijing Key Laboratory of Intelligent Telecommunication Software and Multimedia
Beijing University of Posts and Telecommunications, Beijing, China
{wangyutingbupt, zhengxiaolong, liangliu, mhd}@bupt.edu.cn

***Abstract*—Low Power Wide Area Networks (LPWAN) such as Long Range (LoRa) show great potential in emerging aquatic IoT applications. However, our deployment experience shows that the floating LPWAN suffer significant performance degradation, compared to the static terrestrial deployments. Our measurement results reveal the reason behind this is due to the polarization and directivity of the antenna. The dynamic attitude of a floating node incurs varying signal strength losses, which is ignored by the attitude-oblivious link model adopted in most of the existing methods. When accessing the channel at a misaligned attitude, packet errors can happen. In this paper, we propose an attitude-aware link model that explicitly quantifies the impact of node attitude on link quality. Based on the new model, we propose *PolarTracker*, a novel channel access method for floating LPWAN. *PolarTracker* tracks the node attitude alignment state and schedules the transmissions into the aligned periods with better link quality. We implement a prototype of *PolarTracker* on commercial LoRa platforms and extensively evaluate its performance in various real-world environments. The experimental results show that *PolarTracker* can efficiently improve the packet reception ratio by 48.8%, compared with ALOHA in LoRaWAN.**

I. Introduction

Despite the prosperity of the Internet of Things (IoT) in terrestrial environments including both urban and rural areas, its applications in aquatic environments remain scarce. With the development of Low Power Wide Area Networks (LPWAN) such as LoRa (Long Range) [1], [2], IoT systems begin to be deployed in aquatic environments such as oceans [3], [4], reservoirs [5], and rivers [6]. The nodes equipped with anchors float on the water surface, forming the so-called floating LPWAN. LoRa improves the sensitivity by Chirp Spread Spectrum (CSS) modulation. For example, Semtech chipset SX1278 [7], [8] claims a -148dBm sensitivity and is capable to operate even under the noise floor. Such a high sensitivity can extend the communication range and offer good reliability, showing great potential in floating IoT deployments.

However, in practice, we surprisingly observe a significant performance degradation when migrating the LoRa deployment from the land to the water. In an open water area, with the transmission power (Tx power) of 4dBm, a floating node 0.3km away from the gateway can only achieve a Packet Reception Ratio (PRR) of 64.7%, whereas the terrestrial node at the same distance can obtain 84% PRR. During the experiments, we also observe more violent node sway with a larger magnitude leads to the more severe PRR degradation.

Our further measurement reveals that the reason behind the performance degradation is the attitude-oblivious channel access mechanism inherited from the terrestrial system designs. The antenna of the floating node will change with its attitude, which further brings about the polarization misalignment of the transceiver antennas. The polarization misalignment will result in the signal strength loss. The existing attitude-oblivious link model neglects the non-trivial impact of attitude on the link quality and allows channel access immediately when the transmitter has a packet. The ignorance is unproblematic in terrestrial networks because their nodes usually don't have sharp attitude changes. But for a floating node, the constantly changing attitude will lead to the dynamic additional signal attenuation, resulting in unstable PRR.

How to get reliable performance for the floating LPWAN is still an open problem. Adopting more robust LoRa parameters such as increasing the Tx power or coding rate [9], [10] will lead to poor energy efficiency. For floating networks in open water, energy is often carefully planned without a redundant budget. On the other hand, blind retransmissions [11], [12] consume too much energy but obtain limited improvements because the retransmission can still happen at the misaligned attitude. In a nutshell, these conventional reliability enhancement methods are inefficient because they rely on the attitude-oblivious link model and fail to capture the short-term link quality variations caused by the fast-changing attitude.

To tackle the above problem, a channel access method that can capture the best-aligned attitude is desired. But getting such a method faces the following challenges. First, though we know the polarization misalignment causes signal strength loss, the relationship between the link quality and the floating attitude is still unclear. Besides, the antenna directivity further complicates the relationship. Blurring the impact of attitude on link quality inevitably incurs errors in seizing the channel access opportunities. Second, pinpointing the best channel access timing is challenging in practice. Channel probing is infeasible because the LoRa's long packet transmission time results in a too low probing rate to timely detect the fast-changing link quality. The floating node can sway a wide magnitude within one second. But a LoRa packet can take tens of milliseconds and even seconds, leaving too many undetected attitudes and therefore missing the best opportunity. Third, when designing the channel access methods for the floating LPWAN that desire a long lifetime to reduce the maintenance

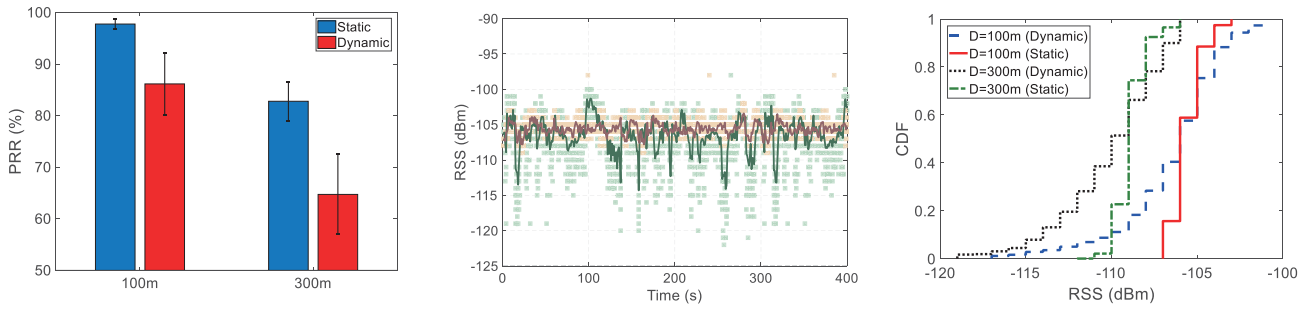

(a) PRR at two distances. (b) RSS changes over time. (c) CDF of RSS.

Fig. 1. The measurement results of the existing method in static and floating environments.

cost, low power consumption should always be kept in mind.

By settling these challenges, we propose *PolarTracker*, an attitude-aware channel access method for the floating LPWAN.

- By thoroughly exploiting antenna polarization and directivity, we conduct real-world observation and discover the relationship between node attitude and signal strength loss. We further propose an attitude-aware link quality model to explicitly quantify the impact of node attitude on link quality, which is a fundamental model that can guide the following system designs in aquatic environments.
- We propose *PolarTracker*, a novel channel access method for the floating LPWAN. *PolarTracker* tracks the dynamic node attitude alignment state and schedules packets into the aligned periods to obtain better link quality. To the best of our knowledge, *PolarTracker* is the first work that discovers and resolves the reliability problem of LPWAN caused by the dynamic attitude in aquatic environments.
- We implement a prototype of *PolarTracker* and extensively evaluate its performance in real-world scenarios. Our evaluation results show that *PolarTracker* can accurately track the aligned attitude and improve the PRR by 1.48×, compared to ALOHA used in LoRaWAN.

The rest of this paper is organized as follows. Section II introduces the background and our measurement of a floating LoRa network, which motivates our work. We then propose the attitude-aware link quality model in Section III and present the designs of *PolarTracker* in Section IV. Evaluation results are shown in Section V. We discuss the related works in Section VI and finally conclude this paper in Section VII.

II. Background and Motivation

In this section, we first briefly introduce the background knowledge and then present the observations of performance degradation when applying LoRa in aquatic environments.

A. Introduction of LoRa and LoRaWAN

LoRa adopts CSS modulation that signal sweeps the whole Bandwidth (BW) and forms a chirp. Spreading Factor (SF) will determine how spread out the chirp is. A larger SF leads to a longer chirp. With other parameters remain unchanged, every increment of SF will double the transmission time of a chirp. Coding Rate (CR) indicates the used redundancy of forwarding error correction code. CR 4/5 means one-bit correction code is added for every four data bits. Transmission power (Tx power) is another important parameter, especially for the floating LoRa networks that demand a long lifetime.

LoRaWAN [1], [13], proposed by the LoRa Alliance, defines a LoRa system architecture and the MAC protocol. LoRaWAN uses the star topology that clients directly transmit data to one or more gateways. LoRaWAN specifies three classes of the MAC protocol, based on the pure ALOHA [14]; that is, LoRaWAN clients will start transmission without any carrier sensing whenever there is a packet.

B. Reliability Degradation of the Floating LoRa Network

To study the performance of floating LoRa, we deploy a LoRa network in a river crossing the suburb area of a city. Two nodes are deployed on the water surface and the gateway is on a bridge 6m above the river. The horizontal distances between the gateway and two nodes are 100m and 300m, respectively. The nodes transmit packets with the Tx power of 4 dBm, using the settings of SF 7, BW 250kHz, and CR 4/5. We measure and compare the PRR of floating nodes and the close-by static terrestrial nodes with the same distance to the gateway.

The PRR results are shown in Fig. 1(a). We surprisingly find that at both distances, the PRR of floating nodes experience obvious degradation, which is up to 64.7% at 300m. Since the only difference between the two experiments is floating nodes sway with the wave, we suspect the dynamic node attitude influences the link quality. To verify our hypothesis, we let the floating and static nodes at 100m continuously transmit packets to the gateway and record the corresponding Received Signal Strength (RSS) no matter the packet has bit errors or not. From the results in Fig. 1(b), we can find that the RSS of the floating node has much larger variations, which can be up to 14dBm. Given such a big RSS drop, it is no wonder the floating node's PRR degrades. In our measurement study, it is not uncommon to encounter RSS drops. From Fig. 1(c), we can find that at both distances, more than 50% of the packets experience obvious RSS degradation.

In the meantime, from the results in Fig. 1(b) and (c), we also observe the phenomenon that floating nodes obtain the comparable and even larger RSS. This observation indicates there are still good transmission opportunities when the node attitude varies. However, the existing attitude-oblivious link model fails discovering and seizing those opportunities. This motivates us to explore a new attitude-aware link model and

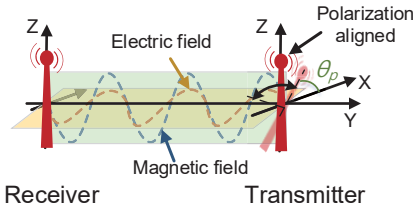

Fig. 2. Illustration of antenna polarization.

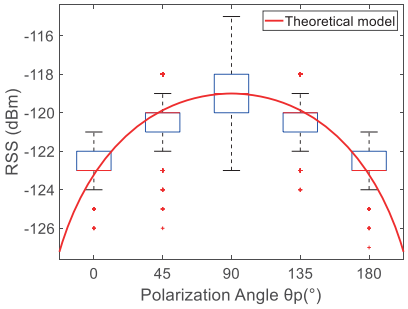

Fig. 3. RSS at different polarization angles.

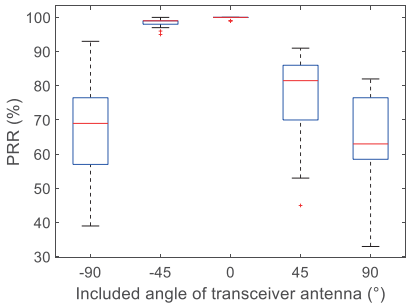

Fig. 4. PRR when swaying in Y-Z plane ($\theta_p = 90°$).

design the corresponding channel access method to solve the reliability degradation problem in the floating LPWAN.

III. Attitude-aware Link Model

To discover and seize the good transmission opportunities, an attitude-aware link model that can quantitatively describe the impact of attitude on link quality is a foremost prerequisite. In this section, by studying the root causes of link quality reduction, we propose the corresponding attitude-aware link model for floating LPWAN.

As we all know, the signal propagates in the air will experience attenuation. The received signal strength P_r can be described by Friis Transmission Formula [15], i.e.,

$$P_r = P_t \frac{G_t G_r \lambda^2}{(4\pi d)^2} \tag{1}$$

where λ is the signal wavelength, d is the distance between the transceiver, G_t and G_r respectively indicate the gains of the transceiver antennas. Frris formula is widely used to analyze communication range and guide the deployments for terrestrial wireless systems.

When reviewing Eq. (1), we notice a fact that the basic Frris formula doesn't explicitly take the transceiver attitude into consideration. However, as shown in Fig. 2, the antennas used in practice are polarized and the electric field has direction. When the receiver antenna deviates the orientation aligned on the electric field, additional signal strength loss will happen. Actually, the basic Friis formula in Eq. (1) has an implicit assumption that polarization between transceiver antennas is aligned. However, in the floating LPWAN, the ever-changing attitude causes the dynamic polarization alignment state. When the transmission happens at the misaligned attitude, additional signal strength loss will cause the RSS drop. Due to the fast-changing attitude, the floating node will experience dynamic drops of RSS and PRR, as observed in Section II.

A. Link Model based on Polarization

The above analysis reveals that the dynamic polarization alignment state caused by an ever-changing attitude is the root cause of PRR degradation of the floating networks. Hence, we try to build the attitude-aware link model based on polarization and include the polarization state into the Friis formula:

$$P_r(\theta_p) = P_t \frac{G_t G_r \lambda^2}{(4\pi d)^2} p \tag{2}$$

where p, Polarization Loss Factor (PLF) [16], [17], is:

$$p = |\overrightarrow{e_r}^* \cdot \overrightarrow{e_t}|^2 = \left|(\cos\theta_p \overrightarrow{x} + \sin\theta_p \overrightarrow{z}) \cdot \overrightarrow{z}\right|^2 = \sin^2\theta_p \tag{3}$$

where θ_p is the polarization angle between transmitter antenna and the X-axis and $(.)^*$ indicates the complex conjugate, $\overrightarrow{e_r}^*$ and $\overrightarrow{e_t}$ are respectively the unit vector of receiver and transmitter antennas. Based on the Reciprocity Theorem of antennas, the transmitting and receiving antenna beams are the same. Hence, without losing generality, the gateway antenna is regarded as vertically upward and we only consider the state of the transmitter antenna.

To verify our model, we conduct experiments with controlled attitudes. For the convenience of controlling attitude, the experiments are done in an open area on the land. We deploy a client $300m$ away from a base station in the same horizontal plane and rotate its antenna along the X-Z plane, as shown in Fig. 2. The client uses the setting of SF 7, BW 250kHz, and CR 4/5. The Tx power is set to 8dBm. We reform the received power in Eq. (2) into RSS (dBm) form, which is $RSS(\theta_p) = 10\lg(P_r(\theta_p)) = RSS(\pi/2) + 10\lg(sin^2(\theta_p))$. The measured RSS at different polarization angles is shown in Fig. 3. We can find the measured RSS results fit the proposed model well.

However, when we apply this model to the deployed floating network, we find packets transmitted at the aligned polarization angle ($\theta_p = 90°$) still get lost. Considering the floating node in the three-dimensional (3D) space also sways in the Y-Z plane, we further measure the PRR when the transceiver antenna tilts different angles in the Y-Z plane. According to the model, when we keep the polarization aligned, we should observe no obvious performance difference. However, from the measured results in Fig. 4, we can clearly find PRR gaps at different angles. Besides, with the same angle deviation, tilting backwards has better PRR than tilting forwards. For example, the average PRR is 98% at $-45°$ but only 77% at $+45°$. The observations indicate that besides polarization, there is another factor of attitude affecting the link quality.

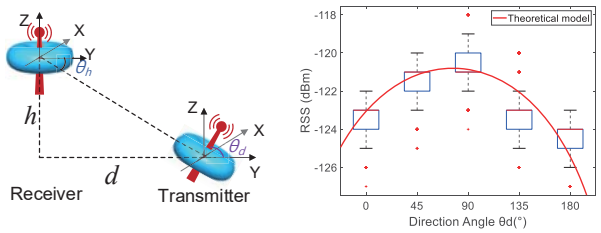

(a) (b)

Fig. 5. Link model when considering antenna directivity with a height difference between the transceiver: (a) Illustration of the antenna directivity, where θ_d and θ_h are the directivity angle and the depression angle; (b) RSS at different directivity angles when the depression angle is fixed.

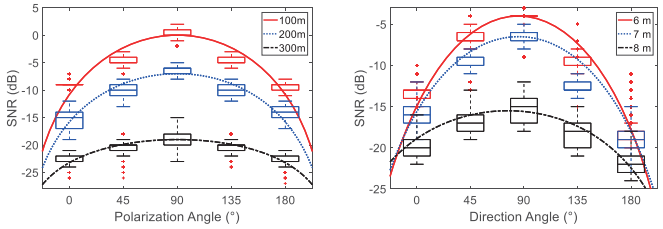

(a) Polarization (b) Directivity

Fig. 6. The attitude impacts at different distances and height differences.

B. Link Model based on Polarization and Directivity

By analyzing the antenna design, we find that the commonly used antenna on IoT devices is the omnidirectional dipole antenna, which has directivity. Instead of spherical radiation, the antenna has a toroidal radiation pattern in 3D space, as shown in Fig. 5(a). The toroidal radiation leads to very little power over and above the antenna. Hence, when there is a height difference between the transceivers, the corresponding depression angle (θ_h in Fig. 5(a)) will incur the directional loss of the received signal strength. The swaying in the Y-Z plane will cause angular variations and exacerbate the loss.

Hence, in the attitude-aware link model, we should take both the polarization and the directivity of the antenna into consideration. For the Frris formula in Eq. (2), we reform G_t and G_r into $\eta_t D_t$ and $\eta_r D_r$, where η_t and η_r are the transceiver antenna efficiency decided by the hardware, D_t and D_r are directivity factors of the transmitter and receiver antennas. The directivity factor [16] is antenna gain in the forward direction divided by the gain in all directions for the omnidirectional antenna, which can be expressed as:

$$D(\theta) = \frac{2f^2(\theta)}{\int_0^{\pi} f^2(\theta)\sin\theta d\theta} \tag{4}$$

where θ represents the angle between the antenna and the direction connecting the transceiver. For the whip antenna used in our application, $f(\theta) = \sin(\theta)$. Since the denominator is definite integral, D equals $a\sin^2(\theta)$, where a is a factor decided by the antenna. In our deployment with the height difference shown in Fig. 5 (a), $D_r = D(\theta_h + \pi/2) = a_r \sin^2(\theta_h + \pi/2)$, where θ_h is the depression angle. When the transmitter sways in the Y-Z plane, $D_t = D(\pi - \theta_h - \theta_d) = a_t \sin^2(\pi - \theta_h - \theta_d)$, where θ_d is the directional angle between the transmitter antenna and the Y-axis. Then the Frris formula in Eq. (2) can be reformed as follows.

$$\begin{aligned} P_r(\theta_p, \theta_d, \theta_h) &= P_t \frac{\eta_t D_t \eta_r D_r \lambda^2}{(4\pi d)^2} p \\ &= P_t \frac{\eta_t \eta_r \lambda^2}{(4\pi d)^2} \sin^2(\theta_p) D(\pi - \theta_h - \theta_d) D(\theta_h + \pi/2) \\ &= P_0 \sin^2(\theta_p) \sin^2(\theta_h + \frac{\pi}{2}) \sin^2(\pi - \theta_d - \theta_h), \end{aligned} \tag{5}$$

where P_0 is the reference signal power that is related to the amplitude of the optimal received signal. Based on Eq. (5), we can obtain the link quality in terms of RSS at the attitude (θ_p, θ_d) as follows.

$$\begin{aligned} RSS(\theta_p, \theta_d, \theta_h) &= 10\lg(P_r(\theta_p, \theta_d, \theta_h)) \\ &= RSS^* + RSS_{PL} + RSS_{DL} + RSS_{HL}, \end{aligned} \tag{6}$$

where RSS^* is the maximum available RSS at a fixed distance between transceiver, obtained when perfectly aligned. RSS_{PL}, RSS_{DL}, and RSS_{HL} are the RSS losses caused by polarization, directivity, and height difference, which are:

$$\begin{aligned} RSS_{PL} &= 10\lg(sin^2(\theta_p)), \\ RSS_{DL} &= 10\lg(sin^2(\pi - \theta_h - \theta_d)), \\ RSS_{HL} &= 10\lg(sin^2(\theta_h + \pi/2)), \end{aligned} \tag{7}$$

We verify this model in our deploying environment. The height of the gateway is $6m$, resulting in $\theta_h = 1.15°$. Since the polarization loss has already been verified, for the convenience of recording ground-truth angles in 3D space, here we control the node attitude only in the Y-Z plane to verify the directivity loss. All the other settings are the same as the verification experiment in Section III-A. The results are shown in Fig. 5(b), which fit well with our model. The RSS is much larger when tilting the same angle forwards to the receiver than backward, which is consistent with the observations in Fig. 4. Due to the height difference, the transmitter antenna's maximum power points to the receiver at the attitudes satisfying $\theta_d + \theta_h = 90°$. Tilting backwards has a chance to satisfy this condition. But keeping the antenna vertical upward in static scenarios can hardly meet this condition. This is why we observe RSS augments during our measurement study in Fig. 1.

We also verify the model at different distances and height differences between the transceivers. We set the Tx power to 4dBm. When varying the distance from $100m$ to $300m$, the height difference is fixed to $6m$. And when varying the height difference from $6m$ to $8m$, the distance between transceivers is fixed to $300m$. The results in Fig. 6 show the Signal-to-Noise Ratio (SNR) which is calculated by the RSS divided by the noise floor. We present SNR to understand the link quality degradation more intuitively. We can find the measured SNR fits the theoretical model very well in Fig. 6. The results verify the effectiveness of the link model based on both polarization and directivity. From the results, we should notice that the model depends on the relative location of the transmitter.

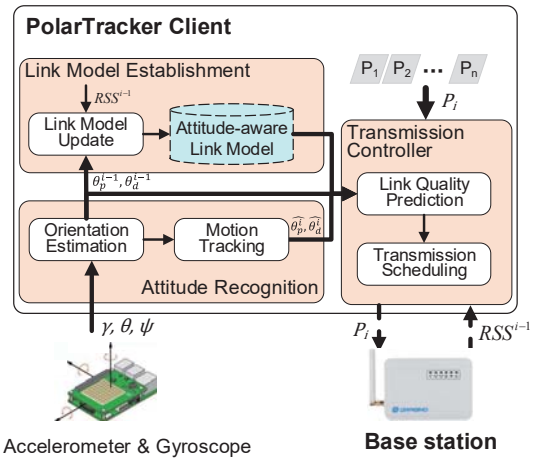

Fig. 7. The overview of *PolarTracker*.

Hence, despite the small probability that the floating node drastically changes its position because of the anchors, we should consider the model update in the design.

Due to the continuity of physical motion, if there is bad transmission timing with poor link quality caused by attitude misalignment, there must be good transmission timing at the aligned attitude. However, due to the wide range and dynamics of the floating node's attitude in 3D space, searching the optimal attitude by probing transmissions at all the angles is infeasible. Obtaining the attitude-aware link model in practice and accordingly utilizing good transmission opportunities still need careful designs.

IV. DESIGN

In this section, based on the attitude-aware link model, we propose a novel channel access method called *PolarTracker* that schedules packets into attitude aligned periods to improve the reliability of the floating LPWAN. We first present an overview of *PolarTracker* and then introduce the major modules.

A. Overview

PolarTracker's design goal is scheduling the channel access into the best-aligned periods to enhance the reliability of floating LPWAN. Even with the knowledge of the theoretical link model, obtaining the optimal fitting model and capturing the optimal attitude in practice is non-trivial. Most of the existing methods are probing based methods that transmit a large number of probing packets to obtain fine-grained RSS measurements covering most of the targeted cases. However, such probing based methods are not suitable for floating LoRa networks. The attitude of the floating node has a wide range in 3D space and changes quickly. The aligned period often lasts only hundreds of milliseconds at a time. But a probing packet in LoRa can take tens of milliseconds and even seconds, resulting in a too low probing rate to timely obtain enough representative RSS samples to fit the model. Besides, probing based methods have a fundamental limitation of acquiring the attitude information. They solely rely on the measured link quality inside the network space but ignore the essential factors behind the phenomenon in physical space.

Instead of using the information in network space only, we utilize the physical attitude information to quickly establish the practical model for each floating node. We can learn from Eq. (5) that if we can obtain the attitude information (θ_p, θ_d) and the corresponding RSS, we can obtain the fitting model by RSS at only a few different attitudes. Therefore, we propose leveraging the on-board Inertial Measurement Unit (IMU) to obtain the physical attitude information. Note that IMU is widely used in floating application systems to collect hydrologic data such as flow rate and flow direction [18], [19]. Hence, reusing the IMU information has no additional hardware or energy overhead. Even if the node has no IMU, adding an IMU has negligible hardware cost ($10 for each) and very limited energy overhead.

Fig. 7 presents the overview of *PolarTracker*, which consists of three main modules: attitude recognition, link model establishment, and transmission controller. Initially, the *PolarTracker* client will use ALOHA in LoRaWAN to access the channel and record the IMU readings with the corresponding RSS. Since IMU provides only Euler angles, *PolarTracker* first estimates the antenna orientation to obtain the polarization angle θ_p and the directivity angle θ_d. Then the attitude (θ_p^i, θ_d^i) when transmitting packet i, along with the RSS^i piggybacked in the ACK from the gateway, is given to the link model establishment module. The model establishment module can estimate the parameters in the attitude-aware link model after accumulating a few measurements. After obtaining the model, the transmission controller comes into effect. With the IMU data, we can track the node motion and predict node attitude in the following short time. By the current attitude and the predicted the next attitude, the link quality prediction module can determine the link quality at the next attitude based on the attitude-aware link model. If a significant RSS drop is predicted, the transmission controller will actively stop the packet transmission to avoid packet loss and resume the transmissions at next alignment. During the transmissions, the *PolarTracker* client can constantly update the model and track the dynamic alignment state.

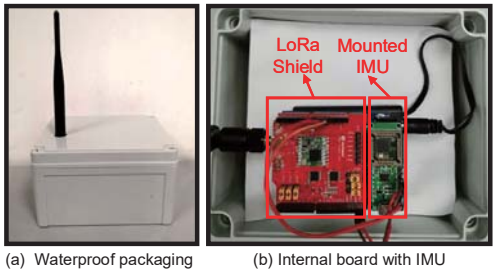

Fig. 8. The client mounted with IMU.

B. Attitude Recognition

To acquire the physical attitude information, we use the IMU fixed on the node board as shown in Fig. 8. Since the antenna is also fixed, its motion is the same as the node motion.

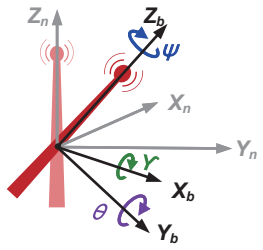

Fig. 9. Antenna sways in 3D space.

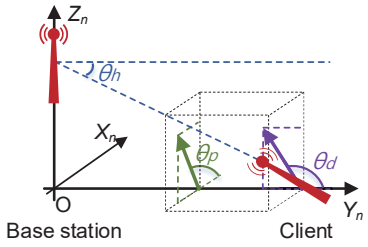

Fig. 10. Illustration of attitude recognition.

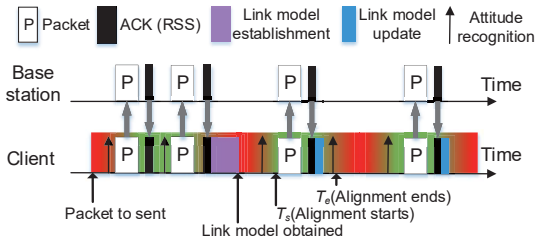

Fig. 11. *PolarTracker* establishes and updates the link model during transmission.

1) Orientation Estimation: As shown in Fig. 9, the IMU provides Euler angles, γ, θ, and ψ, based on its coordinate system $ox_by_bz_b$. Even though the IMU's coordinate system may be different from the geographic coordinate system $ox_ny_nz_n$, their transformation relation is unchanged because the IMU is fixed on the board. We can easily obtain the transformation relation between two coordinates systems before deployment. For conciseness, without losing generality, we assume the two coordinates systems have been calibrated and consistent with each other in the following description.

When node swaying, the IMU coordinate relative to the geographical coordinate in terms of Euler angles can be expressed as:

$$\begin{bmatrix} x_b \\ y_b \\ z_b \end{bmatrix} = \mathrm{C}_n^b(\gamma,\theta,\psi) \begin{bmatrix} x_n \\ y_n \\ z_n \end{bmatrix} \tag{8}$$

where $\mathrm{C}_n^b(\gamma,\theta,\psi)$ is the Direction Cosine Matrix that indicates the relationship between two coordinate systems and can be expressed as follows [20].

$$C_n^b(\gamma,\theta,\psi) = \begin{pmatrix} \cos\psi & \sin\psi & 0 \\ -\sin\psi & \cos\psi & 0 \\ 0 & 0 & 1 \end{pmatrix} \begin{pmatrix} \cos\theta & 0 & \sin\theta \\ 0 & 1 & 0 \\ -\sin\theta & 0 & \cos\theta \end{pmatrix} \begin{pmatrix} 1 & 0 & 0 \\ 0 & \cos\gamma & -\sin\gamma \\ 0 & \sin\gamma & \cos\gamma \end{pmatrix} \tag{9}$$

Then we can obtain the coordinates of the antenna in the geographic coordinate system. As shown in Fig. 10, we can obtain the polarization angle θ_p by projecting the antenna into the X-Z plane and calculating the angle between the projection and the positive X-axis. Similarly, we project the antenna into the Y-Z plane to obtain the directivity angle θ_d.

2) Motion Tracking: Due to the software delay, starting the transmission after detecting a good attitude will lead to a delay of actual channel access, wasting the good transmission time. Hence, predicting the next attitude and loading packet just before the alignment is necessary. Though floating dynamics make the motion hard to model, we can track the short-term antenna motion due to the inertia and continuity of physical motions. In our design, the sampling rate of IMU is 200Hz. The continuous motion is divided into motion slots, each of which lasts 5*ms*. We use the most recent three slots to trace the motion direction and the angular velocity in the last slot as the angular velocity in the next slot. In this way, we can predict the following attitudes for the transmission controller that will be introduced in Section IV-D. Note that the node will sway back after reaching the maximum magnitude, causing sudden direction changes. We can calibrate the predicted attitude by taking the remainder when the calculated results exceed the maximum historical magnitude.

C. Attitude-aware Link Model Establishment and Update

Based on the attitude $(\hat{\theta}_p, \hat{\theta}_d)$ acquired by the attitude recognition module and the corresponding $\hat{RSS}$, we can estimate the parameters in Eq. (6) to obtain the link model for each floating node. The workflow in Fig. 11 presents how *PolarTracker* establishes and updates the attitude-aware link model. Initially, there is no information about the attitude and the link quality. Hence, *PolarTracker* follows LoRaWAN and adopts ALOHA to transmit the packets but records the corresponding attitudes when transmitting packets. We ask the gateway piggybacks the RSS of the received packets in the ACK messages. In this way, the *PolarTracker* client can collect the measured RSS value corresponding to the attitude at time i, i.e, $\{(\hat{\theta}_p^i, \hat{\theta}_d^i), \hat{RSS}^i\}$. In Eq. (6) and Eq. (7), only two parameters, θ_h, and RSS^*, are unknown. After accumulating several measurements, the attitude-aware link model for this floating node at this position can be established.

Due to the limited computing power of low-power LoRa nodes, solving the trigonometric and inverse trigonometric functions is infeasible. Hence, we calculate and store the values of the logarithmic sine function and the values if sine function from 0 to 90° with a step of 1° in advance. When calculating Eq. (7) and Eq. (9), *PolarTracker* directly quires the table using the angles. When we calculate the directivity loss, the directivity angle θ_d will dominate and we can ignore the impact θ_h because it will be much smaller than θ_d in our targeted wide-area deployments where the communication distance is much longer than the height difference. Then *PolarTracker* will schedule and control the packets to be transmitted in the aligned periods. During the following transmissions, more observations of RSS at different attitudes can be continuously accumulated and the model can be constantly updated to adapt to floating dynamics.

For floating LPWAN that have high deployment and maintaining cost, energy efficiency is crucial. Our model establishment and update method is light-weight and highly energy-efficient. The probing-based methods consume too much energy on transmitting probing packets. In LoRa, with a Tx power of 17dBm, the power consumption can be 87mA and

each packet can last for tens or even hundreds of milliseconds. Besides, due to the low achievable probing rate, blind probing has to cover multiple swaying rounds to obtain enough measurements at different attitudes to acquire the best link quality. Different from the probing-based methods, we utilize the low-power IMU sensors to directly acquire the physical attitude information and obtain the RSS measurements from legacy data packets. The power consumption of the IMU sensor is only $280\mu A$ in our current implementation, which is much lower than packet transmissions. Besides, if the application already has used IMU data, we can just reuse the data without extra overhead.

D. Transmission Controller

The goal of the transmission controller module is scheduling the channel access of packets into the aligned periods. The packet transmission has inevitable software delay, including the packet loading, radio state switching, etc. Therefore, if we make the decision after detecting a good aligned attitude, the channel will be accessed with a non-negligible delay that wastes the valuable aligned period. Hence, *PolarTracker* integrates a link quality prediction component to predict the link quality at the next predicted attitude based on the link model and current attitude.

Different from LoRaWAN that accesses the channel immediately when there is a packet, *PolarTracker* proactively controls the channel access time to enhance the reliability. That is, if the predicted link quality is getting better for reliable transmission, *PolarTracker* will schedule the transmission at the next attitude and start loading the next packet into radio in advance.

V. EVALUATION

We extensively evaluate *PolarTracker*'s performance in various real-world scenarios. First, we present the experiment settings and then show the evaluation results in detail.

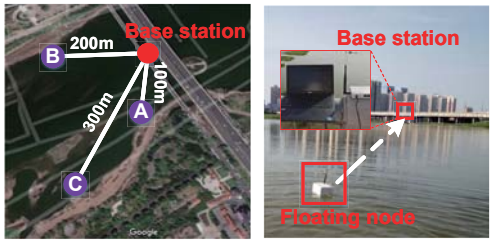

(a) Network deployment (b) Experiment scene

Fig. 12. Experiment settings.

A. Experiment Setup

To evaluate *PolarTracker*, we implement and deploy a prototype system on commercial LoRa platforms with three clients and a gateway, as shown in Fig. 12(a). A Dragino LG01-P LoRa Device with HopeRF's RFM96W [21] is used as the base station. *PolarTracker* is implemented on the commercial Dragino Lora Shield [21] with Semtech SX1278. The gain of the antenna used in our prototype is 3dBi. The network

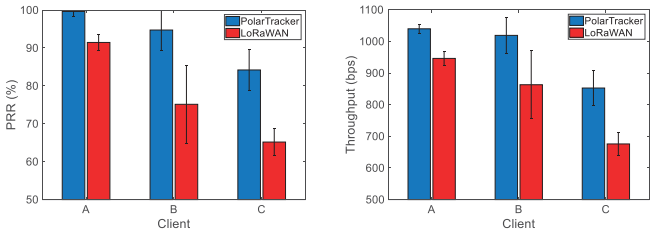

(a) PRR (b) Throughput

Fig. 13. The real-world performance in the aquatic environment.

operates at the $433MHz$ frequency band. During the following experiments, unless otherwise specified, the parameters of LoRa nodes are set as: $SF = 7$, $BW = 250kHz$, and $CR = 4/5$. The length of the packet payload is 8 bytes. When evaluating point-to-point performance, we use client C. The IMU sampling rate is 200Hz. To compare with LoRaWAN, we also implement the ALOHA protocol on our prototype platforms. Fig. 12(b) shows the experiment scene.

B. Real-world Performance in the Aquatic Environment

We first present an overview of the real-world performance of our deployed floating network in the aquatic environment. Fig. 13 shows the PRR and throughput of *PolarTracker* and LoRaWAN of the clients A, B, and C. For all the three clients, *PolarTracker* achieves a better performance. From Fig. 13(a), we can find that the average PRR of *PolarTracker* of three clients are 99%, 94.7%, and 84.2%, while the average PRR of LoRaWAN is 91.4%, 75.1%, and 65.2%. *PolarTracker* is $1.08\times$,$1.26\times$,$1.29\times$ better than LoRaWAN respectively. The throughput is measured by the corrected received bits when transmitting at the highest data rate of LoRa. Similar improvements can be observed. The results demonstrate *PolarTracker* can indeed improve the reliability of floating networks in real-world aquatic environments. In the following, we will further evaluate *PolarTracker* in detail.

C. Impact of LoRa Transmission Parameters

LoRa has multiple parameters that can influence reliability. Hence, we evaluate the performance of *PolarTracker* when LoRa using different parameters to verify *PolarTracker* can improve the performance in different settings. For comparison, we also conduct the experiments using LoRaWAN in static and floating scenarios. During all the experiments, the distance between transceivers is consistent to keep fairness.

1) Impact of Tx Power: The foremost parameter is the Tx power that directly affects the RSS. Hence, we first study the performance of *PolarTracker* when varying the Tx power from 2 to 10dBm. The PRR of the different methods is shown in Fig. 14(a). *PolarTracker* can effectively improve the PRR to the level of LoRaWAN in the static scenario. When Tx power is 2dBm, LoRaWAN can only obtain a PRR of 55.1%, while *PolarTracker* can achieve a PRR of 82% increasing by 48.8%, which is similar to the PRR when LoRaWAN uses a Tx power of 8dBm. From the results, we find that *PolarTracker* can achieve better performance than LoRaWAN

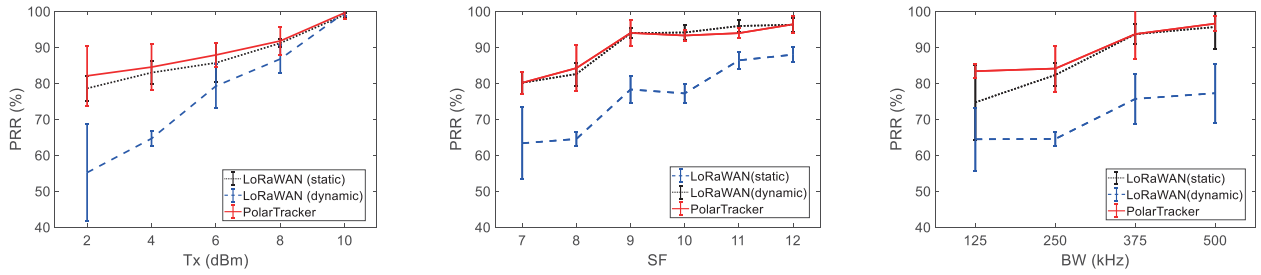

(a) Tx power (b) SF (c) BW

Fig. 14. Performance with different LoRa parameters.

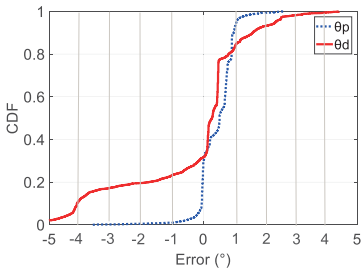

Fig. 15. The accuracy of attitude recognition.

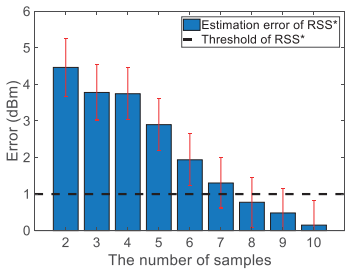

Fig. 16. The accuracy of the link model establishment.

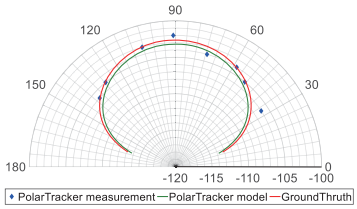

Fig. 17. The fitting curve of *PolarTracker* .

in the static scenario because *PolarTracker* can capture the directivity aligned attitude when swaying backwards.

2) Impact of SF: In LoRa, a chirp consists of a 2^{SF} number of RF chips in a symbol window. Every increment of SF will double the transmission time of a chirp. Increasing SF will lower the sensitivity and have better reliability. Hence, we study the performance of three methods when SF varies from 7 to 12. The experimental results are shown in Fig. 14(b). As expected, with the increase of SF, PRR increases obviously. But at all settings, *PolarTracker* outperforms LoRaWAN. When the SF is 7, the PRR of *PolarTracker* reaches 80%, while the LoRaWAN is only 63.3%. What's worth noticing is the PRR of *PolarTracker* with SF 8 is close to that of LoRaWAN with SF 11. It means *PolarTracker* can use a much lower SF for the floating nodes to obtain the similar PRR, which may bring a potential 8× data rate improvement.

3) Impact of BW: Similar to SF, BW is related to the data rate. We study the performance at commonly used BW 125, 250, and 500kHz. The experiment results are shown in Fig. 14(c). Again, *PolarTracker* achieves the best PRR, which can improve the PRR by up to 30% when using BW 125kHz. We can also find increasing bandwidth can improve reliability for all the methods. Based on our understanding, the reason behind this result is that the larger BW, the shorter on-air time of a packets is, and the less affected by the dynamic attitude.

D. Performance of PolarTracker's Modules

1) Accuracy of Attitude Recognition: We first evaluate the accuracy of the attitude recognition module. We vary the antenna attitude at different angles from 0° to 180° in our lab and measure the calculation errors of θ_p and θ_d based on the IMU data. Fig. 15 shows the Cumulative Distribution Function (CDF) of the estimation errors of θ_p and θ_d. The average errors of θ_p and θ_d are 0.44° and 0.36° respectively. The accuracy is good enough for further link model establishment and transmission control.

2) The Accuracy of Link Model: Though our model can be calculated with only two RSS at different attitudes, more measurements can help improve the accuracy of parameter estimation. Hence, we study the estimation accuracy of RSS^* at a fixed height with varying the numbers of measurements in the deployed network. The parameter estimated by ten-minute measurements is regarded as the ground-truth. The average estimation errors using different the number of measurements are shown in Fig. 16. We can find that the error decreases when using more measurements, as expected. And using eight measurements is good enough to obtain the RSS^* estimation with the error less than 1dBm. Hence, in our current implementation, we use eight measurements to establish the model. We also plot the curve of our fitting model obtained by eight measurements in the view of θ_d in Fig. 17. Note that the link model is obtained by both θ_d and θ_p. We use the view of θ_d only for display clearness. We can find the fitting curve is very close to the ground-truth. The results demonstrate that *PolarTracker* can quickly establish the link model based on only a few measurements.

3) The Accuracy of Capturing the Aligned Attitude: After obtaining the link model, we can capture the aligned attitude based on motion tracking and link quality prediction modules. As previously mentioned, channel probing based methods that transmit at the attitude with the best probed RSS are not accurate due to the low achievable probing rate. We compare

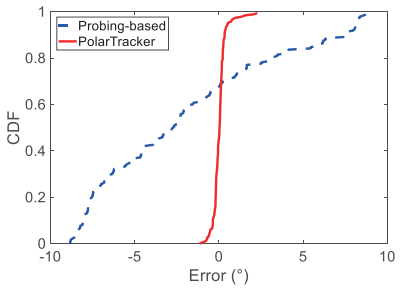

Fig. 18. The accuracy of capturing alignments.

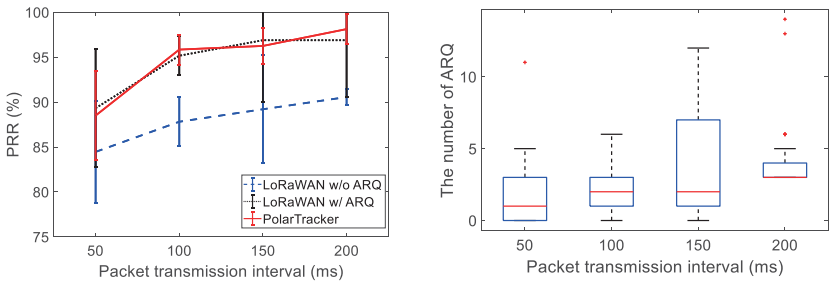

(a) PRR (b) Throughput

Fig. 19. Comparison with the retransmission scheme.

the aligned attitude estimation accuracy of *PolarTracker* and the probing based method based on 20 probing packets sent in one second. The deviations from the best-aligned attitude of two methods are shown in Fig. 18. We can find that *PolarTracker* can capture an aligned attitude with less than 1° error for most of the cases. But the probing based method with error of nearly 10° cannot accurately capture the attitude.

E. Comparison with the Retransmission Scheme

Retransmission is a simple method that resends the lost packets, identical to automatic repeat request (ARQ). But blind retransmissions in floating LPWAN cost too much energy. We compare *PolarTracker* with LoRaWAN augmented with ARQ when the client has different packet rates. The results are shown in Fig. 19. We can find that retransmission can also improve the PRR, obtaining a similar PRR to *PolarTracker*. But the retransmission scheme is to gain the benefit of PRR at the expense of energy consumption. From the results in Fig. 19(b), we can find a large number of retransmissions are needed to obtain the PRR improvements. But *PolarTracker* only needs to transmit once. For the energy-hungry floating LPWAN, the energy-consuming retransmission scheme is unfavored.

VI. Related Work

Despite the prosperity of IoT in terrestrial environments [22]–[25], its applications in aquatic environments remain scarce. But researchers keep attempting to apply IoT in aquatic environments for many years. The early deployments mainly use short-range wireless techniques [26], [27], such as ZigBee in Oceansense [28], WiFi and LTE in [29]. But either the limited communication range or high cost of infrastructure hinders large-scale applications. The emergence of LPWAN brings to light for the floating IoT systems, due to its low cost and long communication range. In recent years, a lot of applications in aquatic environments are proposed [3]–[6].

LoRa with high sensitivity is expected to have good reliability. However, according to our deployment experience, we find the reliability degradation of the floating LoRa network, which has not been discovered and solved. Existing reliability improvement methods used in territorial environments are inefficient to solve this problem. Many existing works focus on controlling the transmission parameters [9], [10], [30] to obtain better PRR but ignore the fact that using more robust parameters can cause unaffordable energy overhead for floating deployments. Similarly, blind retransmissions [11], [12] consume too much energy but obtain limited improvements. A few MAC protocols are proposed to improve the reliability [31]–[33]. For example, LMAC [33] designs three efficient CSMA-based MAC protocols for LoRa networks to balance the loads of the channels defined by frequencies and spreading factors. Further, aiming at the reliability reduction caused by packet collision, a large number of concurrent decoding methods are proposed [34]–[36]. For instance, CoLoRa [35] utilizes packet time offset to disentangle collided packets. Most of the existing works on LPWAN reliability neglect the impact of attitude on link quality and only rely on the in-network probed information to adjust the transmissions. Different from them, we focus on solve the reliability problem caused by the dynamic attitude of the floating nodes in aquatic environments. We propose a novel attitude-aware channel access method based on our new link model.

VII. Conclusion

In this paper, we propose *PolarTracker*, a novel attitude-aware channel access method dedicated to the floating LPWAN. We theoretically establish an attitude-aware link model that quantitatively describes the relationship between the attitude of a floating node and its link quality. Instead of using only in-network probed information, *PolarTracker* also leverages the on-board IMU to directly acquire the physical attitude information and quickly obtain the practical link model with only a few measurements. *PolarTracker* tracks the node attitude alignment state and actively schedules the packets to access the channel during the aligned periods with better link qualities. The extensive experimental results demonstrate the efficiency of *PolarTracker*. In the real-world deployment in aquatic environments, *PolarTracker* can improve the PRR by 48.8%, compared with LoRaWAN.

Acknowledgment

This work is supported in part by NSFC under No. 61722201 and No. 62072050, the Innovation Research Group Project of NSFC under No. 61921003, the International Cooperation and Exchange Project of NSFC under No. 62061146002, and the Fundamental Research Funds for the Central Universities under No. 2019XD-A14.

REFERENCES

[1] N. Sornin, M. Luis, T. Eirich, T. Kramp, and O. Hersent, "Lorawan specification," *LoRa alliance*, 2015.

[2] M. Chen, Y. Miao, Y. Hao, and K. Hwang, "Narrow band internet of things," *IEEE Access*, vol. 5, pp. 20 557–20 577, 2017.

[3] L. Parri, S. Parrino, G. Peruzzi, and A. Pozzebon, "A lorawan network infrastructure for the remote monitoring of offshore sea farms," in *Proceedings of IEEE I2MTC*, 2020.

[4] P. S. Dehda, S. Jayram, A. M. Abu-Mahfouz, and K. Ouahada, "A sea rescue operation system based on lora," in *Proceedings of IEEE International Conference on Advances in Big Data, Computing and Data Communication Systems (icABCD)*, 2019.

[5] W. Du, Z. Xing, M. Li, B. He, L. H. C. Chua, and H. Miao, "Optimal sensor placement and measurement of wind for water quality studies in urban reservoirs," in *Proceedings of IEEE IPSN*, 2014.

[6] J. Cecílio, P. M. Ferreira, and A. Casimiro, "Evaluation of lora technology in flooding prevention scenarios," *MDPI Sensors*, vol. 20, no. 14, p. 4034, 2020.

[7] SX1278, "Datasheet sx1276/77/78/79," 2020. [Online]. Available: https://semtech.my.salesforce.com

[8] L. SX1276, "77/78/79 datasheet." [Online]. Available: http://www.semtech.com/images/datasheet/sx1276

[9] F. Cuomo, M. Campo, A. Caponi, G. Bianchi, G. Rossini, and P. Pisani, "Explora: Extending the performance of lora by suitable spreading factor allocations," in *Proceedings of IEEE WiMob*, 2017.

[10] J. C. Liando, A. Gamage, A. W. Tengourtius, and M. Li, "Known and unknown facts of lora: Experiences from a large-scale measurement study," *ACM Transactions on Sensor Networks (TOSN)*, vol. 15, no. 2, pp. 1–35, 2019.

[11] B. Paul, "A novel mathematical model to evaluate the impact of packet retransmissions in lorawan," *IEEE Sensors Letters*, vol. 4, no. 5, pp. 1–4, 2020.

[12] R. Choi, S. Lee, and S. Lee, "Reliability improvement of lora with arq and relay node," *Symmetry*, vol. 12, no. 4, p. 552, 2020.

[13] L. Alliance, "A technical overview of lora and lorawan," *White paper*, 2015.

[14] N. Abramson, "The aloha system final technical report," *ARPA, contract no. NAS2-6700*, 1974.

[15] R. C. Johnson and H. Jasik, "Antenna engineering handbook," *New York, McGraw-Hill Book Company.*, 1984.

[16] C. A. Balanis, *Antenna theory: analysis and design*. John wiley & sons, 2016.

[17] L. Shangguan and K. Jamieson, "Leveraging electromagnetic polarization in a two-antenna whiteboard in the air," in *Proceedings of ACM CoNEXT*, 2016.

[18] J.-H. Chen, S.-C. Lee, and D. B. DeBra, "Gyroscope free strapdown inertial measurement unit by six linear accelerometers," *Journal of Guidance, Control, and Dynamics*, vol. 17, no. 2, pp. 286–290, 1994.

[27] G. Chen, W. Dong, Z. Zhao, and T. Gu, "Towards accurate corruption estimation in zigbee under cross-technology interference," in *Proceedings of IEEE ICDCS*, 2017.

[19] G. Dissanayake, S. Sukkarieh, E. Nebot, and H. Durrant-Whyte, "The aiding of a low-cost strapdown inertial measurement unit using vehicle model constraints for land vehicle applications," *IEEE transactions on robotics and automation*, vol. 17, no. 5, pp. 731–747, 2001.

[20] A. Mokhtari and A. Benallegue, "Dynamic feedback controller of euler angles and wind parameters estimation for a quadrotor unmanned aerial vehicle," in *Proceedings of IEEE ICRA*, 2004.

[21] "https://www.dragino.com."

[22] H. Li, Y. Gao, W. Dong, and C. Chen, "Bound-based network tomography for inferring interesting link metrics," in *Proceedings of IEEE INFOCOM*, 2020.

[23] W. Dong, C. Cao, X. Zhang, and Y. Gao, "Understanding path reconstruction algorithms in multihop wireless networks," *IEEE/ACM Transactions on Networking*, vol. 27, no. 1, pp. 1–14, 2018.

[24] Y. Peng, L. Shangguan, Y. Hu, Y. Qian, X. Lin, X. Chen, D. Fang, and K. Jamieson, "Plora: A passive long-range data network from ambient lora transmissions," in *Proceedings of ACM SIGCOMM*, 2018.

[25] X. Xia, Y. Zheng, and T. Gu, "Litenap: Downclocking lora reception," in *Proceedings of IEEE INFOCOM*, 2020.

[26] G. Guan, B. Li, Y. Gao, Y. Zhang, J. Bu, and W. Dong, "Tinylink 2.0: integrating device, cloud, and client development for iot applications," in *Proceedings of ACM MobiCom*, 2020.

[28] K. Liu, Z. Yang, M. Li, Z. Guo, Y. Guo, F. Hong, X. Yang, Y. He, Y. Feng, and Y. Liu, "Oceansense: Monitoring the sea with wireless sensor networks," *ACM SIGMOBILE Mobile Computing and Communications Review*, vol. 14, no. 2, pp. 7–9, 2010.

[29] H. Ferreira, F. Silva, P. Sousa, B. Matias, A. Faria, J. Oliveira, J. M. Almeida, A. Martins, and E. Silva, "Autonomous systems in remote areas of the ocean using bluecom+ communication network," in *OCEANS 2017-Anchorage*, 2017, pp. 1–6.

[30] B. Reynders, W. Meert, and S. Pollin, "Power and spreading factor control in low power wide area networks," in *Proceedings of IEEE ICC*, 2017.

[31] B. Reynders, Q. Wang, P. Tuset-Peiro, X. Vilajosana, and S. Pollin, "Improving reliability and scalability of lorawans through lightweight scheduling," *IEEE Internet of Things Journal*, vol. 5, no. 3, pp. 1830–1842, 2018.

[32] D. Zorbas, P. Maillé, B. O'lynn, and C. Douligeris, "Fast and reliable lora-based data transmissions," in *Proceedings of IEEE ISCC*, 2019.

[33] A. Gamage, J. C. Liando, C. Gu, R. Tan, and M. Li, "Lmac: Efficient carrier-sense multiple access for lora," in *Proceedings of ACM MobiCom*, 2020.

[34] X. Xia, Y. Zheng, and T. Gu, "Ftrack: parallel decoding for lora transmissions," in *Proceedings of ACM SenSys*, 2019.

[35] S. Tong, Z. Xu, and J. Wang, "Colora: Enabling multi-packet reception in lora," in *Proceedings of IEEE INFOCOM*, 2020.

[36] X. Wang, L. Kong, L. He, and G. Chen, "mlora: A multi-packet reception protocol in lora networks," in *Proceedings of IEEE ICNP*, 2019.